DESIGN AND OPTIMIZATION OF A VACUUM SYSTEM FOR A LARGE STORAGE TANK CLEANING ROBOT
/
大型贮罐清理机器人吸尘系统的设计与研究

Yong TIAN[1], Zhengtao WANG[2], Jian SONG[1], Fuxiang XIE*[1], Hongwei WANG[1]
[1] School of Machinery and Automation, Weifang University, Shandong/ China;
[2] WindSun Science & Technology Co., Ltd., Shandong / China
Tel: +86-18863637275; E-mail: 20210007@wfu.edu.cn
DOI: https://doi.org/10.35633/inmateh-73-57

Keywords: *Cleaning robot, EDEM, Gas-solid coupling, Structural optimization, Nozzle, Dust suction test*

ABSTRACT
Taking the large storage tank as the cleaning object, a cleaning robot integrating shoveling, crushing, sweeping and dust-absorbing was developed, and its dust-absorbing system was analyzed and optimized. Firstly, Fluent-EDEM gas-solid coupling was utilized to simulate the dust-absorbing system. By analyzing the fluid distribution and particle trajectory, the internal structure of the dust collection box was optimized to reduce the dust particles entering the fan box. Then, by analyzing the structural parameters of the suction nozzle, the influence of the nozzle shoulder angle, nozzle length, and shoulder height on the dust-absorbing effect was explored, and the parameters were determined, so as to reduce the energy loss and increase the flow rate on both sides of the nozzle. Finally, through the dust suction test, different models of nozzles were tested for dust suction, and the wind speed at the nozzle was measured, and the leakage of dust particles on both sides of the nozzle was significantly reduced after optimization, which verified the reliability of the simulation results and provided a theoretical basis for the design of the sweeping robot.

摘要
以大型贮罐作为清理对象，研制了一种集铲装、破碎、清扫、吸尘为一体的清理装置，并对其吸尘系统进行研究。首先，利用 Fluent-EDEM 气固耦合对吸尘装置进行仿真分析，通过对集尘箱中的流体分布和颗粒轨迹进行分析，完成了对集尘箱内部结构进行结构优化，减少了进入风机箱的尘粒；然后，通过对吸嘴结构参数分析，探究了吸嘴肩部夹角、吸嘴长度、肩部高度对吸尘效果影响，确定了吸嘴吸尘性能最佳时的参数，减少了能量损失，增大吸嘴两侧的流速；最后，通过吸尘试验，对不同型号吸嘴进行吸尘测试，将吸尘前后效果进行对比，得出优化后吸嘴两侧漏吸的尘粒明显减少。并对吸嘴处的风速进行测量，将得到结果与仿真数据进行对比，保证了验证仿真的可靠性，从而为清扫机器人的设计提供理论基础。

INTRODUCTION
Currently, there are two main ways of cleaning large storage tanks. One is to utilize robotic arms carrying water spraying devices (*Bogue and Robert, 2011; Buckingham and Graham, 2012; Dandan et al., 2015; Michal, 2012*), and the other way is to utilize cleaning robots (*Anonymous, 2012; Asafa et al., 2018; Azizi and Naderi, 2013; Nesaian and Karthikeyan, 2012; Song et al., 2020*). In this study, a clean-up robot was designed to clean large tanks. As the last part of the cleaning operation, vacuuming collects the residues. In order to avoid secondary processing of the collected dust particles, the vacuuming device is required to not only collect, but also automatically pour the collected dust particles into a collection container.

At present, many researchers have done a lot of studies on the dust suction port used in various occasions, including various studies on the geometry of the dust suction port and the organization of the airflow inside the dust suction port. Chen (*Chen, 2023*) improved the geometric structure of the dust suction port on the basis of the traditional model of dust suction port. In order to increase the working efficiency of the dust suction port, side baffles perpendicular to the wings were added to the edges of the left and right wings, which is conducive to optimizing the direction of airflow through the bottom of the dust suction port, resulting in a smoother flow of airflow and improving the dust removal efficiency. Through the study of the suction port of the vacuum truck, *Walter et al., (2012*), found that changing the traditionally used straight up and down suction port into a new type of suction port with a certain angle had a better control effect on the internal dust-containing airflow, and the streamlined structural design allowed particulate matter to be discharged more quickly.

Yang et al., (2012), analyzed the effect of the extended area outside the suction port on the dust removal performance through simulation experiments, which added a new research direction for the simulation experiments of the suction port.

Some scholars used discrete eddy method to test, and proved that the structural parameters of the dust hood flange length and tilt angle would have an impact on the dust absorption efficiency (*Logachcv et al., 2019*). *Lu et al., (2023*), used a reasonable turbulence model to analyze the factors causing the escape phenomenon and derived the trajectory of particles in industrial production. *Huang, (2016*), used numerical simulation to study the law of gas-solid two-phase flow under high temperature conditions, and found that the height of the dust hood from the heat source was a key factor affecting the escape of high-temperature dust, and proposed to change the dust hood from the heat source height offset and the ventilation of the dust hood could be effective in controlling the escape of high-temperature dust. *Xi et al., (2016*), used Fluent to numerically simulate the gas-solid two-phase flow characteristics inside the dust suction port, and found that the increase of the inclination angle of the front baffle of the dust suction port and the pressure drop of the dust suction port could improve the dust suction efficiency. *Wang and Tan, (2020)*, used Fluent to analyze the working process of the dust extraction hood, and concluded that the height of the dust extraction aperture from the ground and the height of the shoulder of the dust extraction port had an effect on the dust extraction efficiency.

Although a large number of researchers have optimized the inner cavity structure of the suction nozzle (*Guo et al., 2019; Huang et al., 2019; Zhou et al., 2024; Ye, 2023)*, the interaction of the influence of each parameter on the dust removal effect is not considered, and a single study of a certain factor can no longer meet the design requirements. Therefore, based on the dust suction system of the existing robot, Fluent is used to analyze the dust transport law and the influence of the structural parameters of the dust collection box and nozzle on the dust suction effect, to further optimize the structure of the nozzle and the dust collection box and to carry out engineering verification, so as to improve the performance of the dust suction system.

MATERIALS AND METHODS

Robot vacuuming system design

The overall structure of the robot is shown in Fig. 1(a). The residue is pulverized with a crushing device, and then the disturbed residue is sent to the collection container by a shoveling device. Fine particles are absorbed by the vacuuming device and sucked into the dust collection box through the suction nozzle at the bottom of the vehicle, and finally the absorbed residue is poured into the collection container, thus completing the whole residue cleaning and collection work.

As the final part of the cleaning operation, the main task of the dust suction is to clean and collect the residue concentrated by the cleaning. The structure of the dust suction device sketch is shown in Fig. 1(b). The working principle of the dust-absorbing device is to utilize the gas from the suction nozzle into the hose to bring the residual dust particles into the dust collection box, and then the gas passes through the top of the baffle into the fan box and is then discharged by the fan. Dust particles will continue to gather in the mouth of the tube and between the baffle plates.

The design of the nozzle is very important for the whole vacuuming system, and the rationality of the nozzle design largely determines the vacuuming efficiency. The main structural parameters of the nozzle of the vacuuming device designed in this paper are: nozzle outlet area *S*, nozzle length *L*, nozzle width *B*, nozzle height *H* and nozzle shoulder height H_1, shoulder angle α, as shown in Fig. 1(c).

a) the cleaning robot

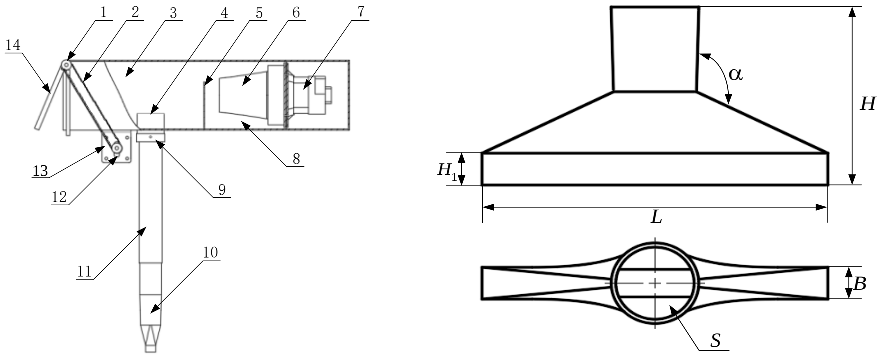

b) Structure of dust suction device; c) Suction nozzle structure

Fig. 1 - Structure of the cleaning robot

1- synchronous wheel, 2-synchronous belt, 3-dust collection box, 4-dust outlet pipe, 5-baffle plate, 6-filter, 7-electric fan, 8-fan box, 9-connecting sleeve, 10-suction nozzle, 11-hose, 12-helm, 13-seat, 14-seal plate

RESULTS

Simulation analysis and optimization of vacuum box

In the simulation, dust particles enter the dust collection box through the suction nozzle and hose. In the simulation process, the particle diameters are set as 0.5 mm, 1 mm, 1.5 mm, 2 mm and 2.5 mm. The number of each kind of particle generation is set to 100. The time step of FLUENT in the simulation process of this paper is set to 1E-04 s, and the number of time steps is 10000.

- Structural analysis of dust collection box

The rationality of the structural design of the dust container is analyzed by Fluent-EDEM coupled simulation (Lin *et al., 2023*). The flow field in Fluent and the particle trajectory in EDEM are combined to analyze the structure of the dust collection box, as shown in Fig. 2(a).

As can be seen from Fig. 2(a), when the gas flow will enter the dust collection box from the pipeline, the gas flow rate at the entrance is obviously higher, and the gas flow is dispersed to both sides when it reaches the upper wall of the box. The gas flow velocity at the upper wall of the box is also significantly higher than other parts. Due to the higher gas flow rate above, the dust particles may cross the baffle plate with the gas flow into the fan box, and the vortex phenomenon appears on both sides of the dust particle inlet. As shown in Fig. 2(b), it can be seen that most of the particles are scattered in the dust collection box, but some of the particles enter into the fan box. The trajectory of the dust particles into the fan box can be clearly seen from the particle trajectory. Based on the velocity vector diagram, it can be seen that particles enter the box from the pipe opening. Due to the wind force of the fan, particles move towards the upper port of the fan box from the outlet.

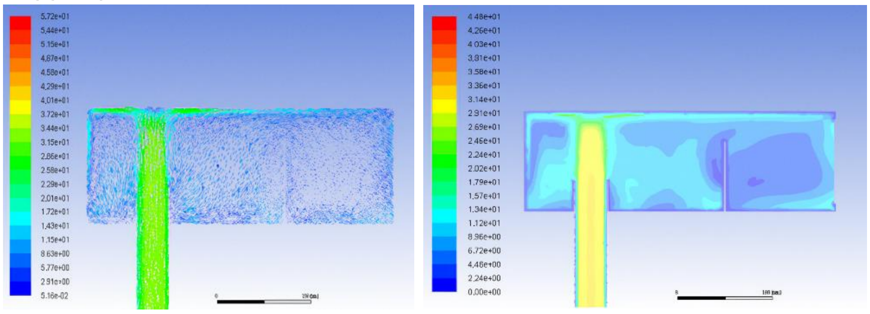

(a) Velocity vector map and cloud

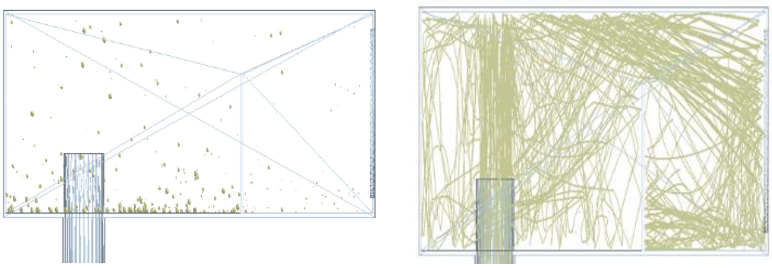

(b) Particle distribution and Trajectories

Fig. 2 - Velocity vector map and cloud

In order to better study the particles entering the blower box, and to provide data support for the subsequent optimization of the dust collection box, the particles entering the blower box are counted, as shown in Table 1. It can be seen that the smaller the particles are, the easier it is to enter the fan box. When the particle diameter is 2.5 mm, the particles entering the fan box obviously become less.

Table 1

Probability of entry of different particles

Particle diameter (mm)	Pre- opt Number (grains)	Post- opt Number (grains)
0.5	57	31
1	30	18
1.5	19	8
2	9	4
2.5	6	0

- Structural optimization of dust collection box

In order to reduce the particles into the fan box, the internal structure of the box is optimized and improved. As shown in Fig. 3, a baffle plate is added above the tube outlet and the inlet of the fan box. When the particles enter the dust collection box from the tube outlet, the particles will slide downward due to the blocking of the plate fixed on the top.

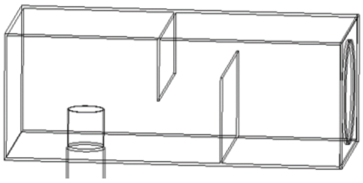

Fig. 3 - Structure of the optimized dust collection box

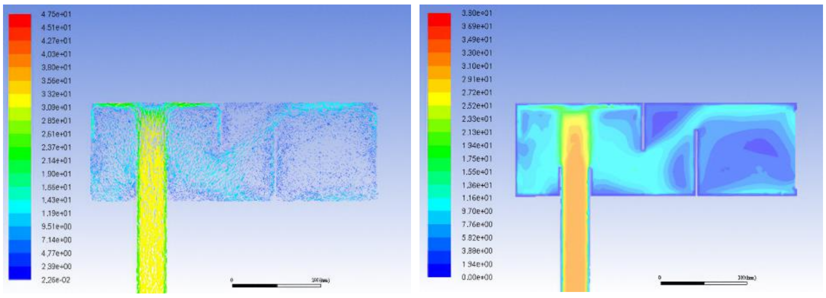

(a) velocity vector map and velocity cloud

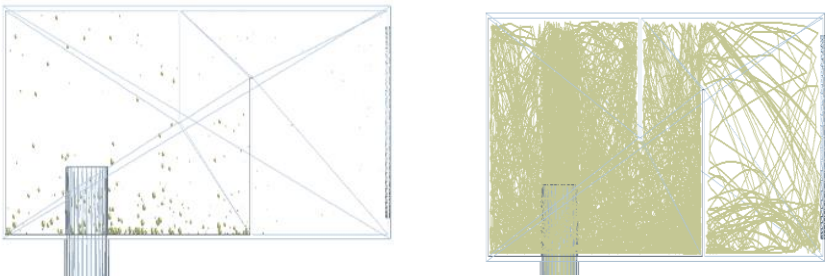

(b) Optimized particle motion trajectories

Fig. 4 - Optimized fluid velocity vector map, velocity cloud and trajectories

The internal structure of the dust collection box is improved, and EDEM analysis is used to obtain the fluid velocity vector map and velocity cloud map inside the box, as shown in Fig. 4(a). From the fluid velocity vector map and velocity cloud diagram, it can be seen that the optimized fluid inside the box changes the direction. As shown in Fig. 4(b), it can be clearly seen that there are more dust particles gathered under the baffle, and the dust particles in the fan box are obviously reduced. The airflow enters into the fan box from the outlet bypassing the baffle plate. When particles reach the baffle from the tube opening, the particles will slide downward due to the existence of the baffle.

By counting the particles in the fan box, the number of different particles entering the fan box is obtained, as shown in Table 1. Comparing with the particles before the optimization analysis, it can be concluded that the quantity of particles entering the fan box is significantly reduced, and the most obvious is the particles with a size of 1.5 mm to 2 mm.

- Structural analysis and optimization of the suction nozzle

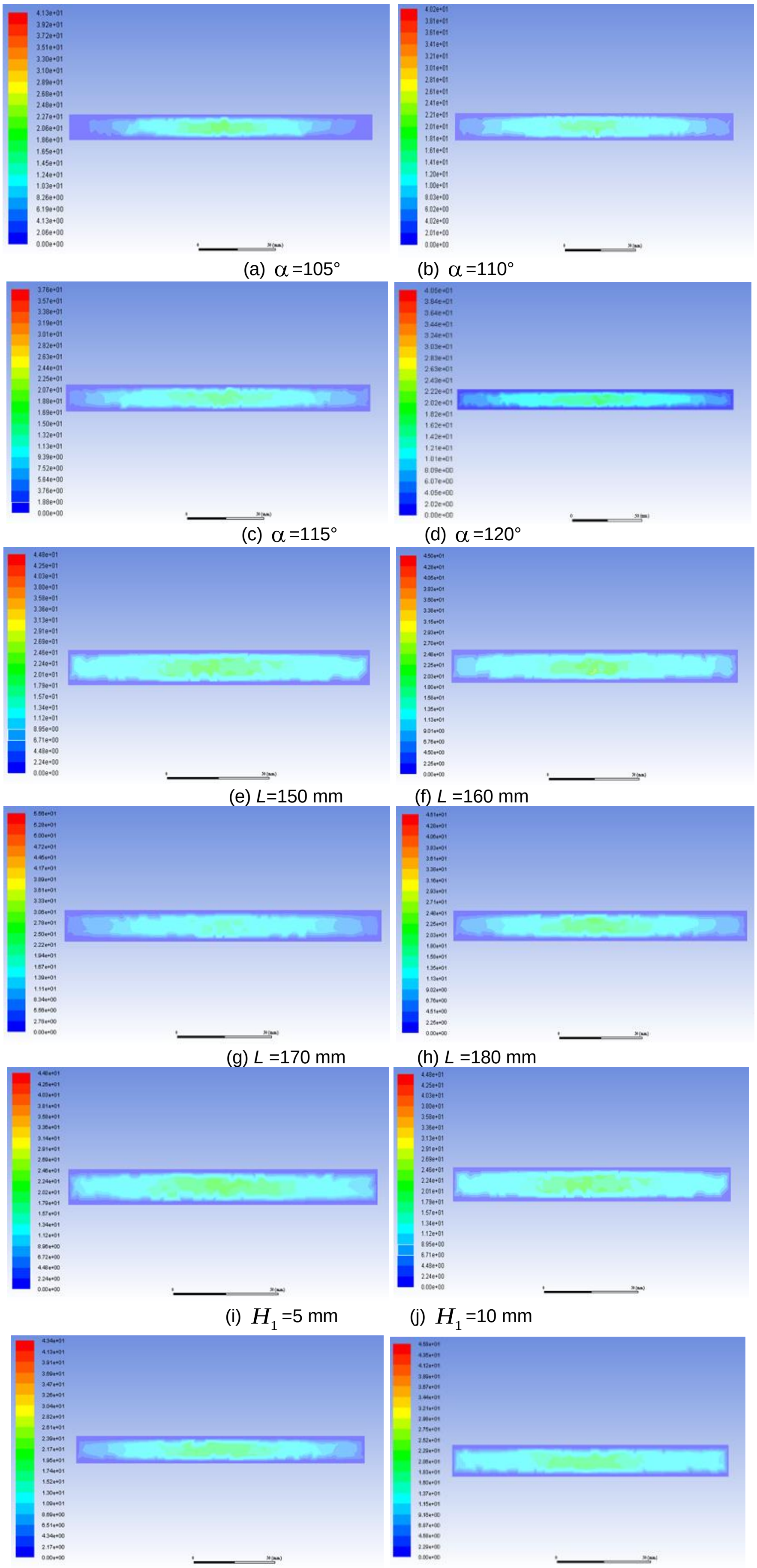

(a) α=105° (b) α=110°

(c) α=115° (d) α=120°

(e) L=150 mm (f) L =160 mm

(g) L =170 mm (h) L =180 mm

(i) H_1 =5 mm (j) H_1 =10 mm

(k) H_1 =15 mm (l) H_1 =20 mm

Fig. 5 - Air velocity distribution at nozzle inlet with different shoulder

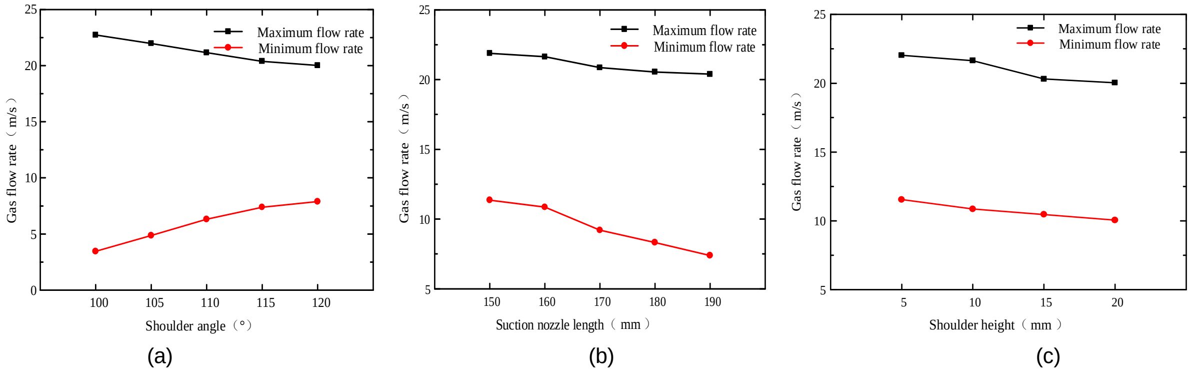

Fig. 6 - Gas flow rate graph

The rationality of the structural design of the suction nozzle is extremely important, and its structural parameters have a great influence on the dust suction efficiency. Through the simulation analysis of the structural design and performance of the nozzle, the stability of the flow field inside the nozzle is ensured.

As shown in Fig. 5(a-d), it can be seen that the flow rate in the center of the nozzle is larger, and the flow rate on both sides is smaller. With the change of the shoulder angle, the yellow area in the center of the nozzle and the light blue area on both sides have different changes, indicating that the shoulder angle has a greater influence on the airflow inside the nozzle. The maximum and minimum values of the gas flow at the entrance of the nozzle were chosen to analyze and compare, and observe the overall change rule of the flow rate under the change of shoulder angle, as shown in Fig. 6(a). The change of the shoulder angle has a greater effect on the flow rate on both sides of the nozzle and a smaller effect on the flow rate in the middle of the nozzle. The maximum and minimum flow velocities show a certain trend when the shoulder angle changes from 105° to 110°, and the change trend becomes smooth from 115° to 120°. The shoulder angle is selected 115° as the optimal parameter in this range.

Figure 5(d-h) shows the effect of changes in nozzle length on the airflow velocity at the nozzle inlet while maintaining a shoulder angle of 115 °. Fig. 6(b) shows that the change of nozzle length mainly affects the gas flow velocity on both sides of the nozzle shoulder, and has less effect on the flow velocity in the middle of the nozzle. The gas flow velocity decreases slowly when the nozzle length is 150 mm to 160 mm, and the gas flow velocity decreases more when the nozzle length is 170 mm to 180 mm. Considering that the nozzle length not only affects the flow rate of the nozzle, but also affects the working width, the nozzle length of 160 mm is selected as the optimal parameter choice.

As shown in Figure 5(i-l), the airflow velocity distribution at the nozzle inlet at different shoulder heights was obtained through simulation, with a shoulder angle of 115 ° and a nozzle length of 160 mm. The airflow velocity values under different shoulder heights are compared and analyzed as shown in Fig. 6(c). It can be found that the maximum and minimum flow velocities show a decreasing trend with the increase of shoulder height. The shoulder height of 5 mm is selected as the optimal choice.

Analysis shows that the maximum and minimum flow rates at the nozzle are the highest when the shoulder angle is 115°, the nozzle length is 160 mm, and the shoulder height is 5 mm. The optimized cross-section of the vacuum device is shown in Fig. 7.

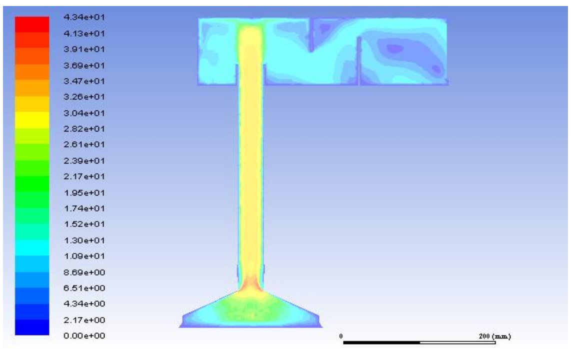

Fig. 7 - Velocity cloud of the optimized vacuum unit

Comparison of the number of dust particles entering the fan box before and after optimization are shown in Table 2. Comparison shows that the optimization of the nozzle structure reduces the number of dust particles entering the fan box, improves the airflow velocity at the nozzle inlet without changing the overall structure, reduces the occurrence of leakage, and improves the efficiency of dust suction.

Table 2

Comparison of data before and after optimization

Projects	pre-opt	post-opt
Percentage of dust particles entering the fan box（%）	31.84	16.05
Maximum velocity of the cross-section at the suction inlet（m/s）	20.01	22.03
Minimum velocity of the cross-section at the suction inlet（m/s）	7.89	11.54
Differential flow rate at the suction port（m/s）	12.12	10.49

Changing the internal structure of the dust collection box reduces the probability of dust particles entering the fan box by 15.75%. The flow rate at the inlet of the nozzle is the largest relative to 22.03 m/s and the minimum flow rate is the largest relative to 11.54 m/s, which can be taken as the optimal choice.

Sample machine test

- Analysis of suction nozzle flow rate

In order to detect the airflow at the entrance of the nozzle, a set of detection points are set up at the entrance of the nozzle to detect the size of the airflow velocity at three points at the entrance. The experimental error is used to analyze the reliability of the simulation results, and the error calculation formula is as follows:

$$\varphi = \left|\frac{H_a - H}{H_a}\right| \times 100\% \tag{1}$$

where, φ is the error, H_a is the experimental value, H is the simulation value.

(a) Dust Extraction Unit Test Stand

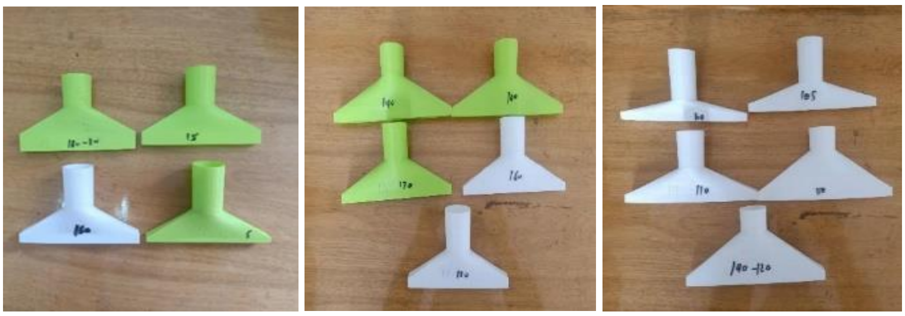

(b) Different height, lengths and angles

Fig. 8 - Dust Extraction Unit Test Stand and different sizes of suction nozzles

As shown in Fig. 8, a speed-adjustable conveyor belt is used to simulate the working conditions when the work is in progress, and the dust particles are evenly spread on the conveyor belt, so that the effect of the suction nozzle in picking up the dust particles can be more clearly observed.

Fig. 8(b) shows suction nozzles with different shoulder heights, different lengths, and different shoulder angles. Measurement points at the inlet of different nozzles were measured.

It can be seen from Table 3 that there are different errors between the measured data and the simulated data for each nozzle. For measurement point 1, the largest error value appears at the nozzle with model number 6, and its error value is 16.43%. For measurement point 2, the largest error occurs at the nozzle with serial number 3, and the error value is 16.72%. For measurement point 3, the largest error occurs at the nozzle of serial number 6, with an error value of 15.56%. The measurement data of the suction nozzle shows the same trend with the simulation data.

Table 3

Data of measurement points

Serial No.	Nozzle type ($\alpha - L - H_1$)	Gas flow speed (m/s)					
		Measurement point 1	Simulation data	Measurement point 2	Simulation data	Measurement point 3	Simulation data
1	100-190-10	9.15	10.82	20.56	22.73	9.68	10.32
2	105-190-10	8.48	10.13	19.69	21.98	8.45	10.15
3	110-190-10	9.36	11.18	18.12	21.15	9.21	11.18
4	115-190-10	9.45	10.62	18.01	20.39	9.45	10.60
5	120-190-10	9.85	11.46	17.46	20.01	9.38	11.45
6	115-150-10	13.33	15.52	19.05	21.89	13.53	15.52
7	115-160-10	13.46	15.18	20.03	21.64	13.58	15.18
8	115-170-10	11.95	13.48	18.98	20.86	11.94	13.95
9	115-180-10	10.21	12.19	18.65	20.55	10.43	12.24
10	115-160-5	14.48	16.46	20.96	22.03	14.48	16.46
11	115-160-15	13.36	15.06	19.23	20.31	13.35	15.06
12	115-160-20	12.03	13.46	18.48	20.03	12.08	13.45

- **Sample machine performance test**

(a) 105-190-5

(b) 115-190-5

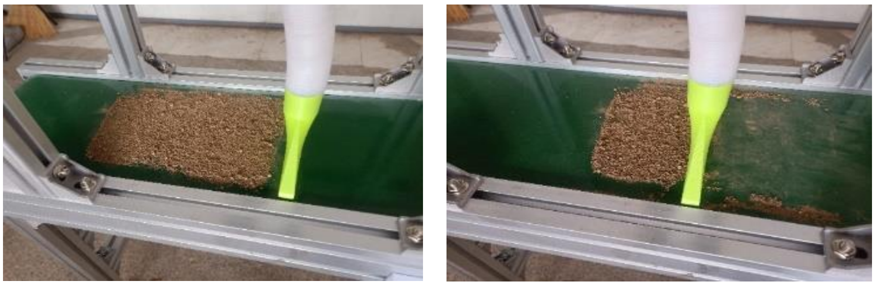

(c) 115-170-5

(d) 115-160-5

Fig. 9 - Comparative test of dust-absorbing effect

A quantity of 50 g of dust particles were taken from the test site and spread evenly on the conveyor belt of the test stand. Two types of nozzles were taken from the two parameters to analyze and compare. Take the suction nozzle model were 105-190-5, 115-190-5, 115-170-5, 115-160-5 as the object of the test. The speed of the conveyor belt was set to 0.1 m/s to simulate the forward speed of the cleaning robot, and the distance between the nozzle inlet and the conveyor belt was set to 10 mm. The effectiveness of different models of nozzles was investigated by observing the distribution of dust particles on the conveyor belt.

As shown in Fig. 9, the effect of the nozzles before and after vacuuming can be clearly seen from the conveyor belt. In Fig. 9(a) (b) (c), the nozzles all have the phenomenon of leakage of dust particles on both sides, and the degree of leakage on both sides of the nozzles is different with the change of the shoulder angle and nozzle length. Fig. 9(d) shows the optimized vacuuming effect, compared with other models of nozzles, there is no leakage of dust particles on both sides.

CONCLUSIONS

(1) The structure of the dust collection box was optimized. Through the comparative analysis of the data before and after the optimization, the dust particles entering the fan box were reduced by 15.75%.

(2) The shoulder angle optimal parameters were selected to increase the gas flow rate to improve the dust suction efficiency.

(3) Through the performance test of the cleaning robot, it was concluded that the leakage of dust particles on both sides of the suction nozzle was obviously improved.

ACKNOWLEDGEMENT

This research has received support from the Weifang Science and technology development plan project (2022GX005).

REFERENCES

[1] Anonymous, (2012). Subsea 7 adds more Schilling Robotics HD Systems to ROV fleet. *Ocean News & Technology,* Vol. 18, pp. 58, USA.

[2] Asafa, T., Afonja, T, Olaniyan, E., & Alade, H., (2018). Development of a vacuum cleaner robot. *Alexandria Engineering Journal*, Vol. 57, pp. 2911-2920, Egypt.

[3] Azizi, M. R., & Naderi, D., (2013). Dynamic modeling and trajectory planning for a mobile spherical robot with a 3dof inner mechanism. *Mechanism & Machine Theory*, Vol. 64, pp. 251-261, Netherlands.

[4] Bogue, & Robert, (2011). Robots in the nuclear industry: a review of technologies and applications. *Industrial Robot*, Vol. 38, pp. 113-118, United Kingdom.

[5] Buckingham, R., & Graham, A., (2012). Nuclear snake-arm robots. *Industrial Robot*, Vol. 39, pp. 6-11, United Kingdom.

[6] Chen, Y., (2023). *Optimization of aerodynamic performance and internal flow characteristics of high-speed centrifugal fans for vacuum cleaners (吸尘器用高速离心式风机气动性能优化及内部流动特性研究)*. Master dissertation, Zhejiang University of Science and Technology, Zhejiang/China.

[7] Dandan, K., Albitar, H., Ananiev, A., & Kalaykov, I., (2015). Motion control of siro: the silo cleaning robot. *International Journal of Advanced Robotic Systems*, Vol. 12, pp. 1, Australia.

[8] Guo, H., Zhang, Z., & Ma, Y., (2019). Structure analysis and improvement of suction nozzle of sweeper （洗扫车吸嘴结构分析及改进）. *Development & Innovation of Machinery & Electrical Products*, Vol. 32, pp. 22-24, Beijing/China.

[9] Huang, X., (2016). *Analysis and experimental research on underwater foreign object salvage robot system for nuclear reactor （核反应堆水下异物打捞机器人系统分析与实验研究）*. PhD dissertation, Hebei University of Technology, Tianjin/China.

[10] Huang, X., Ye, J., & Xiong, J., (2019). Optimized design and test of suction nozzle of small sweeper（小型清扫车吸嘴的优化设计与试验）. *Machine Design & Research*, Vol. 35, pp. 168-172, Shanghai/China.

[11] Lin, H., Xu, C., & Lu, Y., (2023). Simulation test and verification of material conveying for small and medium-sized air suction jujube picking machine based on CFD-DEM coupling （基于 CFD-DEM 耦合中小型气吸红枣捡拾机物料输送仿真试验与验证）. *INMATEH - Agricultural Engineering*, Vol. 71, pp. 535-547, Romania.

[12] Logachcv, K.I., Ziganshin, A.M.， & Averkova, O.A., (2019). On the resistance of a round exhaust hood shaped by outlines of the vortex zones occurring at its inlet. *Building and Environment.* Vol. 151, pp. 338-347, United Kingdom.

[13] Lu, Y., Zhang, B., & Chen, Z., (2023). Numerical simulation and optimization design of sweeper suction nozzle flow field (清扫车吸嘴流场仿真分析及优化设计). *Construction Machinery Technology & Management*, Vol. 4, pp. 75-78, Beijing/China.

[14] Michal, V., (2012). Remote operation and robotics technologies in nuclear decommissioning projects-ScienceDirect. *Nuclear Decommissioning*, pp. 346-374, Netherlands.

[15] Nesaian, K. P., & Karthikeyan, M. B., (2012). Design and development of vision based blockage clearance robot for sewer pipes. *IAES International Journal of Robotics & Automation*, Vol. 1, pp. 64-68, USA.

[16] Song, Z., Zhou, C., & Zhang, S., (2020). Application of dredging robot in culvert dredging project （清淤机器人在暗涵疏浚工程中的应用）. *Northwest Hydropower*, Vol. 4, pp.70-73, Shanxi/China.

[17] Walter, S., Ulli-Beer, S., & Wokaun, A., (2012). Assessing customer preferences for hydrogen-powered street sweepers: a choice experiment. *International Journal of Hydrogen Energy*, Vol. 37, pp. 12003-12014, United Kingdom.

[18] Wang, G., & Tan, Y., (2020). Structural optimization design of vacuum hood based on FLUENT-EDEM coupling （基于 FLUENT-EDEM 耦合的吸尘罩结构优化设计）. *Journal of Vacuum Science and Technology*, Vol. 40, pp. 66-80, Beijing/China.

[19] Xi, Y., Cheng, K., & Lou, X., (2016). Numerical analysis of the flow field of a blowback nozzle and study of dust suction efficiency （反吹式吸嘴流场数值分析及吸尘效率研究）. *Journal of Southwest Jiaotong University*, Vol. 51, pp. 105-112, Sichuan/China.

[20] Yang, C., Zhang, Y., & Yang, Z., (2012). Parameter design of vacuum cleaner suction port based on fluent simulation （基于流畅模拟得真空清扫车吸尘口的参数设计）. *Journal of Central South University*, Vol. 09, pp. 3704-3710, Hunan/China.

[21] Ye, J., (2023). *Structure Research and Performance Analysis of vacuum port of pure electric small sweeper (纯电动小型扫地车吸尘口结构研究与性能分析).* Master dissertation, Anhui University of Technology, Anhui/China.

[22] Zhou, H., Zhang, C., Liu, T., Wang, Y., Fang, J., & Hu, A., (2024). Design and experiment of annular air-blowing assisted seed guiding device for corn no-till planter (玉米免耕播种机环形气吹辅助导种装置设计与试验). *INMATEH - Agricultural Engineering*, Vol. 73, pp. 50-62, Romania.